PLOS | ONE

RESEARCH ARTICLE

Optical Properties of Ferroelectric Epitaxial $K_{0.5}Na_{0.5}NbO_3$ Films in Visible to Ultraviolet Range

E. Chernova[1,2]*, O. Pacherova[1], T. Kocourek[1], M. Jelinek[1], A. Dejneka[1], M. Tyunina[1,3]*

1 Institute of Physics of the Czech Academy of Sciences, Na Slovance 2, Prague 8, Czech Republic, 18221, **2** Czech Technical University, Technicka 2, Prague 6, Czech Republic, 166 27, **3** Microelectronics and Materials Physics Laboratories, University of Oulu, P. O. Box 4500, FI-90014 Oulun yliopisto, Finland

* chernova@fzu.cz (EC); marinat@ee.oulu.fi (MT)

Citation: Chernova E, Pacherova O, Kocourek T, Jelinek M, Dejneka A, Tyunina M (2016) Optical Properties of Ferroelectric Epitaxial $K_{0.5}Na_{0.5}NbO_3$ Films in Visible to Ultraviolet Range. PLoS ONE 11(4): e0153261. doi:10.1371/journal.pone.0153261

Editor: Sefer Bora Lisesivdin, Gazi University, TURKEY

Received: January 26, 2016

Accepted: March 26, 2016

Published: April 13, 2016

Data Availability Statement: All relevant data are within the paper and its Supporting Information files.

Funding: This work was supported by Czech Science Foundation (Grant No. 15-13778S, https://gacr.cz, recipient: AD) and Finnish Funding Agency for Innovation (Grant No. 400.31.2013, https://www.tekes.fi/en, recipient: MT).

Competing Interests: The authors have declared that no competing interests exist.

Abstract

The complex index of refraction in the spectral range of 0.74 to 4.5 eV is studied by variable-angle spectroscopic ellipsometry in ferroelectric $K_{0.5}Na_{0.5}NbO_3$ films. The 20-nm-thick cube-on-cube-type epitaxial films are grown on $SrTiO_3$(001) and $DyScO_3$(011) single-crystal substrates. The films are transparent and exhibit a significant difference between refractive indices Δn = 0.5 at photon energies below 3 eV. The energies of optical transitions are in the range of 3.15–4.30 eV and differ by 0.2–0.3 eV in these films. The observed behavior is discussed in terms of lattice strain and strain-induced ferroelectric polarization in epitaxial perovskite oxide films.

Introduction

Perovskite-structure oxide ferroelectric crystals have long been used for optical applications due to their good nonlinear optical properties, high transparency and large index of refraction in the visible range [1, 2]. Advanced integrated optoelectronic and photonic applications can be implemented using thin single-crystal epitaxial films instead of bulk crystals [3–6]. However, epitaxial growth of ferroelectric films on dissimilar substrates is known to result in different phases of the crystal and electronic structures as well as ferroelectric polarization; such behavior is significantly different from those of bulk prototype crystals [7–10]. Correspondingly, the optical properties of epitaxial ferroelectric films can differ from those of the crystals [11, 12]. Knowledge of the epitaxial effects on the optical properties is vital for emerging thin-film ferroelectric applications.

Here, we experimentally study the optical properties of epitaxial ferroelectric $K_{0.5}Na_{0.5}NbO_3$ (KNNO) films. Recent intensive research on bulk ceramic KNNO has been stimulated by the excellent piezoelectric properties of this solid solution, which is an environmentally friendly alternative to traditional lead-containing piezoelectrics [13]. In addition, potential optical applications of KNNO have been explored [14–17]. The room-temperature crystal structure of KNNO was identified as monoclinic [18]. By growing KNNO on top of a cubic substrate, it is

possible to induce tetragonal crystal symmetry and lattice strain in the KNNO film. Here, such films are obtained using $SrTiO_3$ and $DyScO_3$ substrates. Our experiments reveal significant difference between the optical properties of these films. The observations are discussed in terms of lattice strain and strain-induced ferroelectric polarization in the films.

Experiment

Epitaxial KNNO films with thickness of approximately 20 nm were grown via pulsed laser deposition on $SrTiO_3$ (001) and $DyScO_3$ (011) single-crystal substrates. The substrate temperature of 700°C and oxygen pressure of 20 Pa were maintained during deposition, and the oxygen pressure was 800 Pa during post-deposition cooling. The room-temperature crystal structure of the films was studied by x-ray diffraction (XRD) on a Bruker D8 DISCOVER SUPER SPEED SOLUTION diffractometer using the Cu-Kα radiation. The lattice parameters were estimated from the positions of Bragg diffractions using EVA software and taking substrates as a reference.

The optical properties of the films were investigated by variable-angle spectroscopic ellipsometry on a VUV J. A. Woollam ellipsometer. Ellipsometric angles ψ and δ were measured at a photon energy range from 0.74 to 4.5 eV with a step of 0.02 eV. The measurements were performed in the reflection mode at multiple incidence angles in the range from 60° to 75° at room temperature. The obtained ellipsometric spectra were analyzed using a WVASE32 software package [19]. As a reference, the $SrTiO_3$ and $DyScO_3$ substrates were inspected independently under similar conditions. The optical constants of the substrates extracted using a model of semi-infinite substrate considering surface roughness, and ambient air are presented in Fig 1. The optical constants of the films were determined using a four-phase model that includes a semi-infinite substrate, one homogeneous layer, surface roughness, and ambient air. The optical constants of the substrate were kept as fixed parameters, and the thickness and oscillator parameters of the films were used as variables in the fitting procedure. The dielectric functions of the films were obtained using the Generalized Oscillator Model in the WVASE 32 software package [19, 20]. An analytical multi-oscillator model was first employed to determine the initial dielectric function and layer thicknesses. The obtained thicknesses of the films were in a good agreement with those determined by XRD analysis. To increase the accuracy of the data fitting procedure in weakly absorbing region [21] we additionally used the numerical inversion to extract optical constants over the full measured spectral range. This approach limits its sensitivity to surface roughness as the absorbing region of the material at higher photon energies is ignored. Such fitting was done with the fixed thickness. The surface roughness was represented as a mixture of 50% solid and 50% voids, according Effective Medium Approximation [22]. The estimated thickness of the surface roughness layer was less than 2 nm for the KNNO thin-film samples.

Results and Discussion

Epitaxy

Cube-on-cube-type epitaxial growth of the KNNO films is revealed by XRD analysis. The Θ-2Θ scans show that the films are perovskite, highly oriented, with the (00*l*) planes parallel to the (001) planes of STO and (011) planes of DSO (Fig 2a–2d). The presence of Laue satellites indicates the high crystal quality of the KNNO films. The thickness of the films estimated from the Laue diffractions is approximately 20 nm. The reciprocal space maps inspected around (303) and $(30\bar{3})$ diffractions of STO and (336) and $(33\bar{6})$ diffractions of DSO evidence in-plane epitaxy with the [100] directions of KNNO being parallel to the [100] directions of STO and to

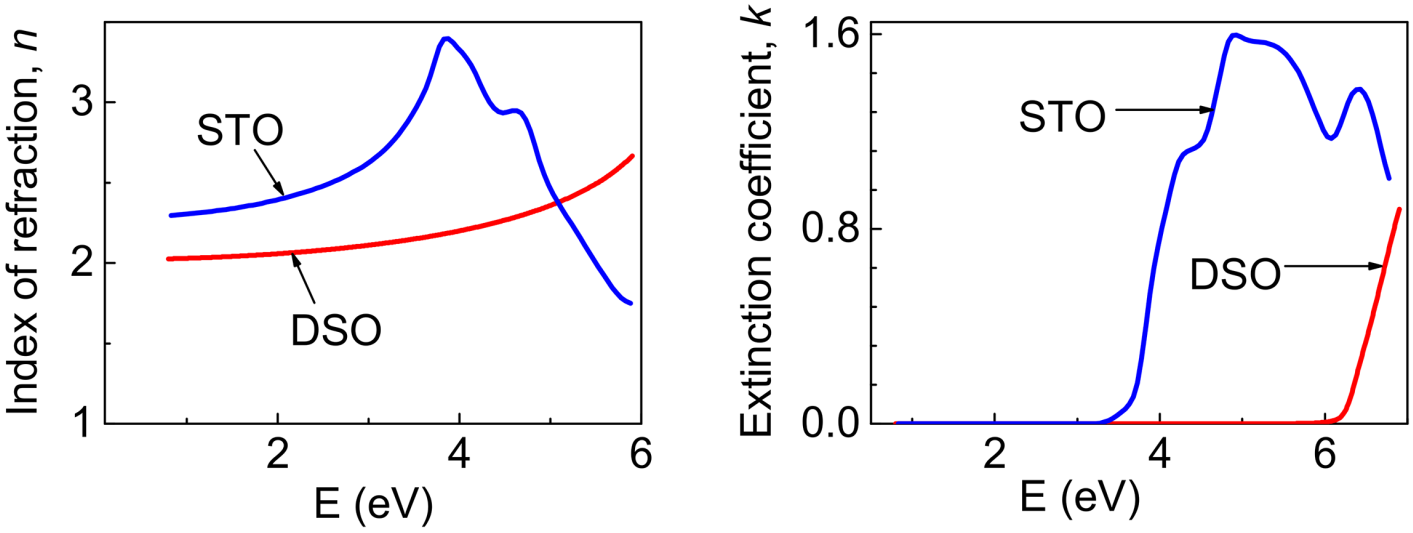

Fig 1. Index of refraction (a) and Extinction coefficient (b) of $SrTiO_3$ and $DyScO_3$ substrates.

doi:10.1371/journal.pone.0153261.g001

the [110] directions of DSO. The out-of-plane and in-plane lattice parameters, c and a, respectively, are found to be c = 3.991Å and a = 3.931Å in the KNNO film on STO, and c = 3.968Å, a = 3.976Å in the KNNO film on DSO. The crystal structure of the KNNO film on STO can be interpreted as tetragonal with the longer out-of-plane lattice parameter ($c > a$) (Fig 3a). Compared to the monoclinic unit cell in the KNNO ceramics [18], the epitaxial KNNO films possess different crystal structures, lattice parameters, and unit cell volumes (Table 1). To estimate lattice strain in the films, the lattice parameter a_0 of a prototype cubic KNNO cell is calculated as $a_0 = V^{1/3} = (a_b\, b_b\, c_b)^{1/3}$, where a_b, b_b, and c_b are the lattice parameters of bulk KNNO. The films

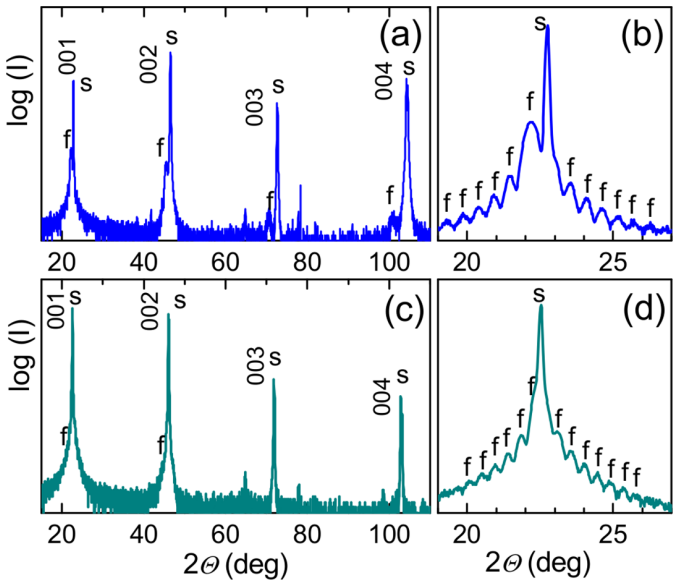

Fig 2. Θ-2Θ x-ray diffraction patterns in the KNNO films on (a,b) $SrTiO_3$(001) and (c,d) $DyScO_3$(011) substrates. Diffractions from the substrates and films are marked by *s* and *f*, correspondingly. Panels (b,d) show scans around (002) diffractions.

doi:10.1371/journal.pone.0153261.g002

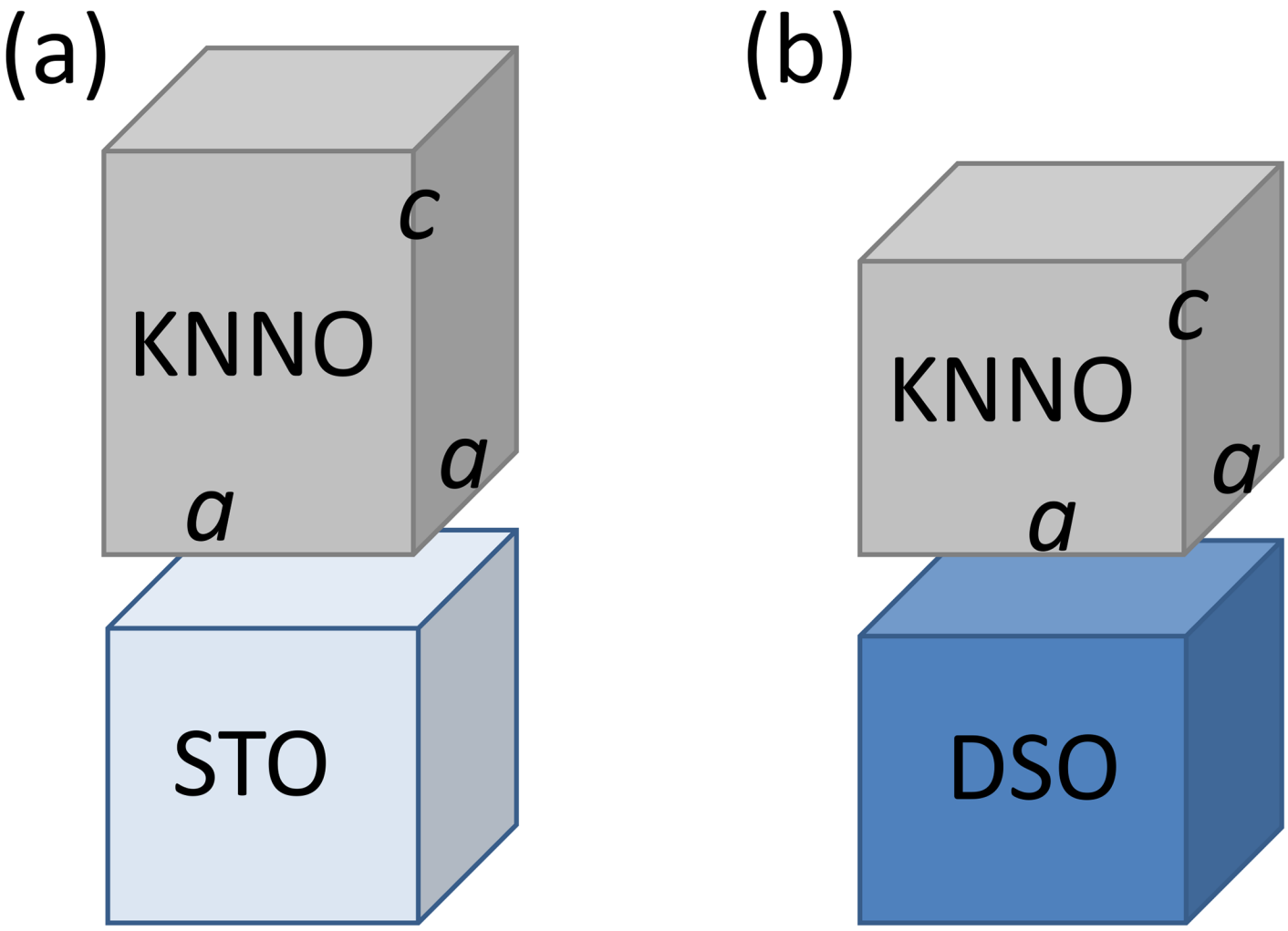

Fig 3. Schematic pesentation of (a) tetragonal and (b) pseudo-cubic unit cells in the cube-on-cube-type epitaxial KNNO films on (a) STO and (b) DSO substrates.

doi:10.1371/journal.pone.0153261.g003

Table 1. Summary of structural and optical properties in ceramics and thin-film KNNO.

	Ceramics [18]	KNNO on STO	KNNO on DSO
Structure	monoclinic	tetragonal	pseudo-cubic
a(Å)	4.0046	3.931	3.976
b(Å)	3.9446	3.931	3.976
c(Å)	4.002	3.991	3.968
c/*a*	—	1.015	0.998
$V(Å^3)$	63.22	61.67	62.73
n (at 2 eV)	—	1.6	2.12
E_0 ($\alpha = 10^4$ cm^{-1}) (eV)	—	3.72	3.55
E_i (indirect) (eV)	—	3.53±0.02	3.15±0.02
E_d (direct) (eV)	—	4.08±0.02	4.30±0.02

doi:10.1371/journal.pone.0153261.t001

experience biaxial compressive in-plane strain $s = a/a_0-1$, which is large ($\sim 1.3\%$) in the KNNO/STO and close to zero (0.1%) in the KNNO/DSO. Considering theoretical phase diagrams of epitaxial $KNbO_3$ and $NaNbO_3$ films [8], the ferroelectric *c*-phase and *r*-phase can exist in the KNNO films on STO and DSO, respectively. The phases differ in the directions and magnitudes of ferroelectric polarization. Next, we show that this differences can lead to dramatic differences in the optical properties of the films.

Optical properties

The complex index of refraction $n^* = n + ik$ is determined in the KNNO films at room temperature. The extinction coefficient k is close to zero over a wide spectral range (Fig 4a). The results show that the films exhibit high transparency in the visible optical range, which is important for applications. The spectra of the refractive index $n(E)$ in Fig 4b agree with those typically observed in the transparency range in perovskite oxide ferroelectrics [23]. In addition, the magnitude of n in the KNNO film on DSO is close to the typical values. However, the refractive index n is dramatically suppressed in the KNNO film on STO. The difference between refractive indices in the KNNO films is huge: the difference is approximately$\Delta n = 0.5$. Note that KNNO belongs to a family of perovskite oxide ferroelectrics, where *d* orbitals of *A*-site cations contribute to electronic band structure (e.g., $BaTiO_3$, but not $PbTiO_3$). The refractive index is connected with electrical polarization through quadratic electro-optic effect in such materials [24]. A semi-empirical relationship is valid in the transparency range, far from edge of absorption:

$$\Delta\left(\frac{1}{n^2}\right) \approx gP^2 \tag{1}$$

Here, the difference $\Delta(1/n^2)$ is taken in relation to the paraelectric state with zero polarization, P is the polarization in the ferroelectric state, and g is the quadratic electro-optic coefficient. The tensor nature of the coefficient g is ignored in expression (1) for simplicity. The coefficient n decreases with increasing spontaneous ferroelectric and/or electric-field-induced polarization. The observed huge difference between the coefficients n in the KNNO films can be caused by different polarization therein. As is known, a strong coupling between lattice

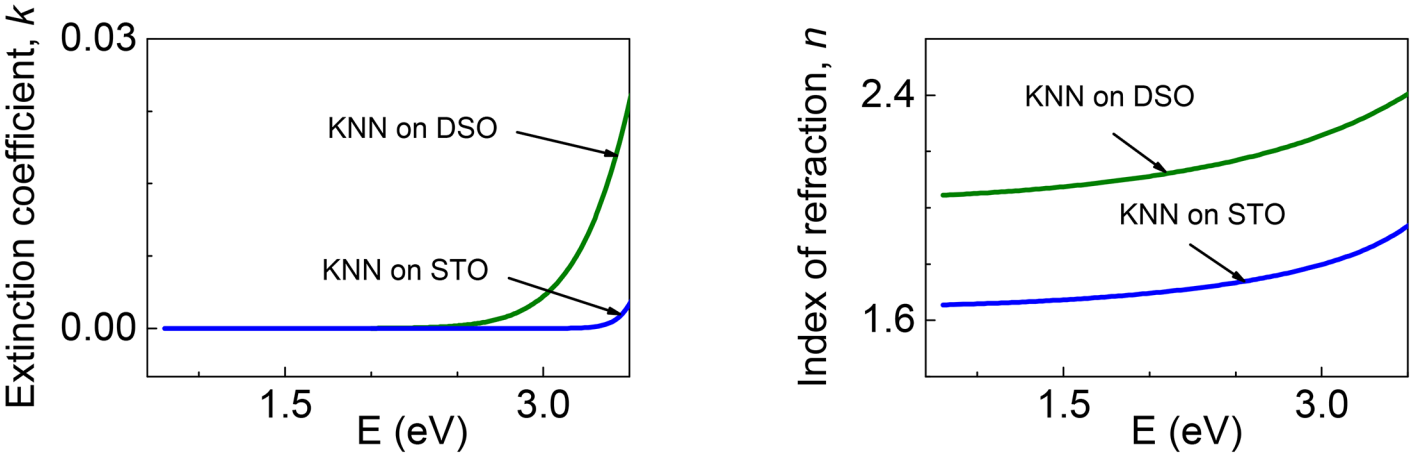

Fig 4. (a) Extinction coefficient *k* and (b) refractive index *n* of KNNO films.

doi:10.1371/journal.pone.0153261.g004

strain and polarization is the characteristic feature of perovskite oxide ferroelectrics. Compared to the KNNO film on DSO, the larger lattice strain causes larger polarization, which, in turn, leads to smaller index of refraction n in the KNNO film on STO.

The microscopic mechanism behind the expression (1) is connected with an increase of electron band energies, especially of valence-band energies, which is induced by polarization in ferroelectrics [23]. The increase of valence-band energy can manifest itself in a widening of the band gap and an increase of the energies of interband optical transitions. Correspondingly, shifts of absorption edge and other spectral features to higher photon energies, i.e., blue shifts, are expected with increasing ferroelectric polarization. To detect such shifts and thus verify the suggested influence of strain-induced ferroelectric polarization on index of refraction in the KNNO film, the spectra of optical absorption $\alpha(E)$ are analyzed (Figs 5 and 6).

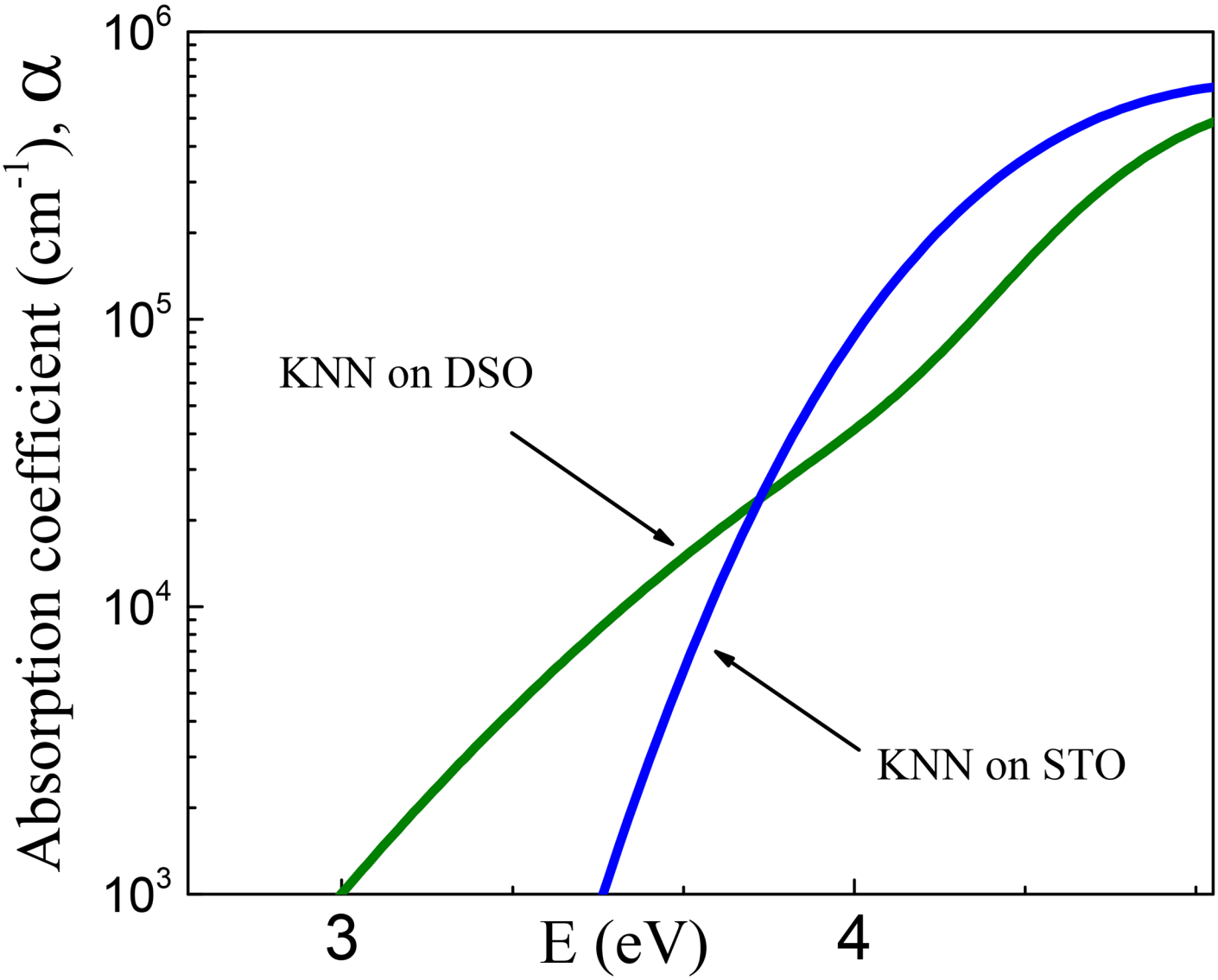

Fig 5. Absorption coefficient α as a function of photon energy E in the KNNO films.

doi:10.1371/journal.pone.0153261.g005

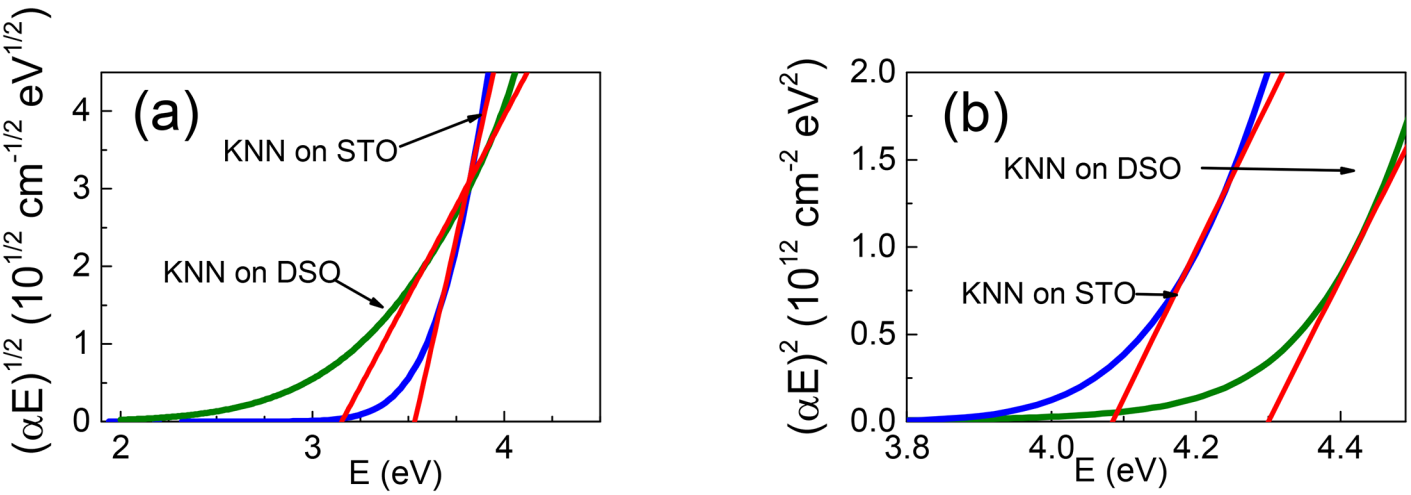

Fig 6. Tauc plots for (a) indirect and (b) direct optical transitions in the KNNO films.

doi:10.1371/journal.pone.0153261.g006

Often, the optical band gap is determined from Urbach tail [25], where $\alpha(E)$ decreases exponentially with decreasing E below energy gap [26]:

$$\alpha(E) = \alpha_0 exp\left[\frac{(E - E_t)}{E_u}\right] \quad (2)$$

Here, E_u describes the slope of absorption tail, E_t is the energy, below which the Urbach behavior is observed, and E_g is the band-gap energy. As seen from Fig 4, the logarithmic plots of absorption coefficient α cannot be fit by a linear function corresponding to the expression (2). The absorption in the KNNO films is free of Urbach tails. Simultaneously, one can notice a clear difference between the spectra in the two films.

To quantify this difference, we use the energy E_α, at which absorption coefficient is $\alpha = 10^4$ cm^{-1}. The energy is $E_\alpha = 3.55$ eV in the film on DSO, and it is larger, $E_\alpha = 3.72$ eV, in the film on STO. The observed blue-shift of absorption edge in the film on STO with respect to that in the film on DSO is consistent with the above-discussed effect of strain-induced polarization. The effect of polarization is further verified by comparing energies of optical transitions in the films.

The energies of transitions are determined using the widely employed Tauc relations [27]. The Tauc plots for both indirect and direct transitions are analyzed. The analysis reveals indirect bandgapin the films (Fig 5a). The bandgap energy E_i is obtained from the linear fits to $[(\alpha E)^{1/2} \propto E]$ in the range of $\alpha = (2\text{-}45)\times10^3$ cm^{-1}. Again, the bandgap energy $E_i = 3.53$ eV in the film on STO is clearly larger than the bandgap energy $E_i = 3.15$ eV in the film on DSO. This result is consistent with the suggested effect of strain-induced polarization.

In addition, good linear fits to $[(\alpha E)^2 \propto E]$ for $\alpha = (1\text{-}3)\times10^5$ cm^{-1} (Fig 6b) evidence the presence of a direct optical transition with the energy E_d in both of the KNNO films. The energy is $E_d = 4.08$ eV in the film on STO, which is smaller than the energy $E_d = 4.30$ eV in the film on DSO. Thus, in contrast to the polarization-caused blue shift of the indirect transition, the higher-energy direct transition is found to red-shift with increasing lattice strain (and, hence, with strain-induced polarization) in KNNO. The observed controversial behavior of optical transitions suggests more complex changes in the band structure. In particular, besides the suggested polarization-induced increase of valence-band energies, band splitting can be

caused by ferroelectric polarization [28]. Such splitting may be responsible for the apparent red-shift of E_d.

Theoretical analysis of optical properties in strained epitaxial ferroelectric films is highly desirable to understand such large variations in behavior as those observed in the present and other works [29–31]. Nevertheless, despite the lack of theoretical support, our experimental results strongly suggest that optical refraction and absorption can be tuned using epitaxial growth of ferroelectric films. The epitaxial-deposition induced changes of optical properties can be employed in creating materials for advanced optoelectronic and photonic applications.

Conclusion

The complex index of refraction in the spectral range of 0.74 to 4.5 eV is studied in 20-nm-thick cube-on-cube-type epitaxial films of ferroelectric $K_{0.5}Na_{0.5}NbO_3$. The films are grown on $SrTiO_3$ (001) and $DyScO_3$ (011) single-crystal substrates, and experience biaxial in-plane compressive strain. Compared to the weakly strained film on $DyScO_3$ (011), the strongly strained film on $SrTiO_3$ (001) exhibits a smaller refractive index in the transparency range and a larger bandgap energy. The observed behavior is explained using a semi-empirical model of the electro-optic effect in ferroelectrics and considering strain-induced polarization in epitaxial films. The results are important for the development of materials for future optoelectronics and photonics.

Author Contributions

Conceived and designed the experiments: AD MT. Performed the experiments: EC OP. Analyzed the data: EC OP. Contributed reagents/materials/analysis tools: TK MJ. Wrote the paper: EC MT.

References

1. Lines ME, Glass AM. Principles and applications of ferroelectrics and related materials. Oxford University Press; 1977.
2. Tejuca LG, Fierro J. Properties and applications of perovskite-type oxides. CRC Press; 2000.
3. Guo R, You L, Zhou Y, Lim ZS, Zou X, Chen L, et al. Non-volatile memory based on the ferroelectric photovoltaic effect. Nature communications. 2013; 4. doi: 10.1038/ncomms2990
4. Dicken MJ, Sweatlock LA, Pacifici D, Lezec HJ, Bhattacharya K, Atwater HA. Electrooptic modulation in thin film barium titanate plasmonic interferometers. Nano letters. 2008; 8(11):4048–4052. doi: 10.1021/nl802981q PMID: 18847247
5. Abel S, Stöferle T, Marchiori C, Rossel C, Rossell MD, Erni R, et al. A strong electro-optically active lead-free ferroelectric integrated on silicon. Nature communications. 2013; 4:1671. doi: 10.1038/ncomms2695 PMID: 23575675
6. Qin M, Yao K, Liang YC. High efficient photovoltaics in nanoscaled ferroelectric thin films. Applied Physics Letters. 2008; 93(12):122904. doi: 10.1063/1.2990754
7. Pertsev N, Zembilgotov A, Tagantsev A. Effect of mechanical boundary conditions on phase diagrams of epitaxial ferroelectric thin films. Physical review letters. 1998; 80(9):1988. doi: 10.1103/PhysRevLett.80.1988
8. Diéguez O, Rabe KM, Vanderbilt D. First-principles study of epitaxial strain in perovskites. Physical Review B. 2005; 72(14):144101. doi: 10.1103/PhysRevB.72.144101
9. Pertsev N, Dkhil B. Strain sensitivity of polarization in perovskite ferroelectrics. Applied Physics Letters. 2008; 93(12):2903. doi: 10.1063/1.2988263
10. Ederer C, Spaldin NA. Effect of epitaxial strain on the spontaneous polarization of thin film ferroelectrics. Physical review letters. 2005; 95(25):257601. doi: 10.1103/PhysRevLett.95.257601 PMID: 16384507
11. Berger RF, Fennie CJ, Neaton JB. Band Gap and Edge Engineering via Ferroic Distortion and Anisotropic Strain: The Case of $SrTiO_3$. Physical review letters. 2011; 107(14):146804. doi: 10.1103/PhysRevLett.107.146804 PMID: 22107228

12. Wang F, Grinberg I, Rappe AM. Band gap engineering strategy via polarization rotation in perovskite ferroelectrics. Applied Physics Letters. 2014; 104(15):152903. doi: 10.1063/1.4871707
13. Saito Y, Takao H, Tani T, Nonoyama T, Takatori K, Homma T, et al. Lead-free piezoceramics. Nature. 2004; 432(7013):84–87. doi: 10.1038/nature03028 PMID: 15516921
14. Sun H, Peng D, Wang X, Tang M, Zhang Q, Yao X. Green and red emission for $(K_{0.5}Na_{0.5})NbO_3$: Pr ceramics. Journal of Applied Physics. 2012; 111(4):046102. doi: 10.1063/1.3686193
15. Wu X, Chung TH, Kwok KW. Enhanced visible and mid-IR emissions in Er/Yb-codoped $K_{0.5}Na_{0.5}NbO_3$ ferroelectric ceramics. Ceramics International. 2015; 41(10, Part B):14041–14048. doi: 10.1016/j.ceramint.2015.07.018
16. Blomqvist M, Khartsev S, Grishin A, Petraru A, Buchal C. Optical waveguiding in magnetron-sputtered $Na_{0.5}K_{0.5}NbO_3$ thin films on sapphire substrates. Applied physics letters. 2003; 82(3):439–441. doi: 10.1063/1.1539295
17. Kroupa J, Petzelt J, Malic B, Kosec M. Electro-optic properties of KNN-STO lead-free ceramics. Journal of Physics D: Applied Physics. 2005; 38(5):679. doi: 10.1088/0022-3727/38/5/003
18. Tellier J, Malic B, Dkhil B, Jenko D, Cilensek J, Kosec M. Crystal structure and phase transitions of sodium potassium niobate perovskites. Solid State Sciences. 2009; 11(2):320–324. doi: 10.1016/j.solidstatesciences.2008.07.011
19. Woollam JA, Hilfiker JN, Tiwald TE, Bungay CL, Synowicki RA, Meyer DE, et al. Variable angle spectroscopic ellipsometry in the vacuum ultraviolet. In: International Symposium on Optical Science and Technology. International Society for Optics and Photonics; 2000. p. 197–205.
20. Woollam J. Guide to Using WVASE32 Spectroscopic Ellipsomtry Data Acquisition and Analysis Software. JA Woollam Co., Inc.; 2005.
21. Gautam LK, Haneef H, Junda MM, John DBS, Podraza NJ. Approach for extracting complex dielectric function spectra in weakly-absorbing regions. Thin Solid Films. 2014; 571, Part 3:548–553. 6th International Conference on Spectroscopic Ellipsometry (ICSE-VI). doi: 10.1016/j.tsf.2014.03.020
22. Fujiwara H, Koh J, Rovira PI, Collins RW. Assessment of effective-medium theories in the analysis of nucleation and microscopic surface roughness evolution for semiconductor thin films. Phys Rev B. 2000 Apr; 61:10832–10844. doi: 10.1103/PhysRevB.61.10832
23. DiDomenico M Jr, Wemple S. Optical properties of perovskite oxides in their paraelectric and ferroelectric phases. Physical Review. 1968; 166(2):565. doi: 10.1103/PhysRev.166.565
24. Wemple S. Polarization Fluctuations and the Optical-Absorption Edge in $BaTiO_3$. Physical Review B. 1970; 2(7):2679. doi: 10.1103/PhysRevB.2.2679
25. Dow JD, Redfield D. Theory of exponential absorption edges in ionic and covalent solids. Physical Review Letters. 1971; 26(13):762. doi: 10.1103/PhysRevLett.26.762
26. Tompkins H, Irene EA. Handbook of ellipsometry. William Andrew; 2005.
27. Tauc J, Grigorovici R, Vancu A. Optical Properties and Electronic Structure of Amorphous Germanium. physica status solidi (b). 1966; 15(2):627–637. doi: 10.1002/pssb.19660150224
28. Brews J. Energy band changes in perovskites due to lattice polarization. Physical Review Letters. 1967; 18(16):662. doi: 10.1103/PhysRevLett.18.662
29. Tyunina M, Yao L, Chvostova D, Kocourek T, Jelinek M, Dejneka A, et al. Effect of epitaxy on interband transitions in ferroelectric $KNbO_3$. New Journal of Physics. 2015; 17(4):043048. doi: 10.1088/1367-2630/17/4/043048
30. Tyunina M, Yao L, Chvostova D, Dejneka A, Kocourek T, Jelinek M, et al. Concurrent bandgap narrowing and polarization enhancement in epitaxial ferroelectric nanofilms. Science and Technology of Advanced Materials. 2015; 16(2):026002. doi: 10.1088/1468-6996/16/2/026002
31. Chernova E, Pacherova O, Chvostova D, Dejneka A, Kocourek T, Jelinek M, et al. Strain-controlled optical absorption in epitaxial ferroelectric $BaTiO_3$ films. Applied Physics Letters. 2015; 106 (19):192903. doi: 10.1063/1.4921083